Oxidation Ability of Plasmon-Induced Charge Separation Evaluated on the Basis of Surface Hydroxylation of Gold Nanoparticles

Hiroyasu Nishi and Tetsu Tatsuma*

Abstract: The oxidation ability of plasmonic photocatalysts, which has its origins in plasmon-induced charge separation and has not yet been studied quantitatively and systematically, is important for designing practical photocatalytic systems. Oxidation ability was investigated on the basis of surface hydroxylation of Au nanoparticles on TiO$_2$ at various irradiation wavelengths and electrolyte pH values. The reaction proceeds only when the sum of the flat band potential of TiO$_2$ and the irradiated photon energy is close to, or more positive than, the theoretical potential for the reaction.

$\mathbf{P}$lasmonic nanoparticles (NPs) trap photons in the visible and near-infrared (NIR) regions on the basis of localized surface plasmon resonance (LSPR). A photon is converted to a plasmon and subsequently to heat or light, which is observed as light absorption or scattering, respectively.[1] In other cases, a plasmon excites a dye molecule or a semiconductor via an optical near-field generated around the resonant NP[2] or resonant energy transfer[3] (nanoantenna effect). Meanwhile, we reported plasmon-induced charge separation (PICS) for the first time, which involves electron injection from a resonant NP to a semiconductor in contact with the particle,[4] and it has been studied extensively.[4–19] PICS can induce various electrical or electrochemical processes in which plasmonic NPs and a semiconductor work as a photoanode and a photocathode, respectively. It has therefore been applied to photovoltaics,[4–7] photocatalysts,[4,8–14] photochromic display devices,[15–17] photoactuators,[18] and potentiometric or conductometric LSPR sensors.[19] In particular, photocatalysis based on PICS attracts much attention, and has been used for photooxidation of alcohols,[4,8] carboxylic acids,[9] and benzene,[10] as well as reduction or oxidation of water into hydrogen[11,13] or oxygen,[11,12,14] respectively. To construct various systems of plasmonic photocatalysis, cathodic and anodic photopotentials of PICS are important. Although the cathodic potential corresponds to the conduction band level of the semiconductor,[4] the anodic potential has not yet been evaluated quantitatively and systematically. Herein, we evaluate dependence of the anodic photopotential of Au NPs deposited on TiO$_2$ (which is the most typical PICS system) on the pH value and incident photon energy, through observation of surface hydroxylation of Au NPs. We demonstrate that the present results for the hydroxylation and previous results for

coordinative dissolution of Au NPs[20] can be explained consistently if the potential is dictated by the sum of flat band potential of TiO$_2$ (E_{fb}) and irradiated photon energy ($h\nu$). These insights would facilitate design of plasmonic photocatalysts and novel photofunctional materials.

We previously examined changes in the surface potential distribution of TiO$_2$ modified with Au nanoplates upon photoirradiation by Kelvin probe force microscopy (KFM) and qualitatively clarified that the surface potential of Au is more positive than TiO$_2$ upon exposure to visible-NIR light; this is consistent with electron injection from Au to TiO$_2$ by PICS.[21] However, quantitative evaluation of the potential has not yet been achieved because of a small amount of adsorbed water on TiO$_2$, which is necessary to retain the band structure of TiO$_2$. An alternative way to evaluate the oxidation ability of PICS is to examine oxidation reactions with known electrode potentials. Although a lot of photocatalytic reactions based on PICS have been reported, as described above, detection sensitivity of reactants and products is not high enough. We previously employed coordinative dissolution of plasmonic Au NPs[17,20] because LSPR is very sensitive to changes in the NP itself. In general, Au is electrochemically stable ($E^\circ_{Au^{3+}/Au} = 1.52$ V)[22] and shows sufficient stability even in PICS.[4] However, in the presence of ligands such as halide ions, Au–ligand complex is formed, resulting in oxidative dissolution of Au at more negative potentials.[17,20,22] We investigated coordinative dissolution of Au NPs deposited on TiO$_2$ in the presence of chloride ions, in particular the dependence on pH value, which affects E_{fb} and $h\nu$. We found that the oxidation reaction proceeds only when $E_{fb} + h\nu$ is more positive than the standard potential for the [AuCl$_4$]$^-$/Au couple ($E^\circ_{[AuCl_4]^-/Au} = 1.00$ V). There are two possible explanations for this: 1) the anodic potential of PICS is $E_{fb} + h\nu$ because electrons are pumped up from the Au NP to the TiO$_2$ conduction band at E_{fb}, and the Fermi level of Au NP is lowered until the Schottky barrier height (ϕ_B) becomes approximately equal to $h\nu$ (Figure 1); 2) a PICS-based oxidation occurs by electron transition from a pH-independent defect level that is slightly more positive than $E_{[AuCl_4]^-/Au}$ (which is independent of pH) to the TiO$_2$ conduction band at E_{fb}. Therefore, herein we employ the surface hydroxylation of Au, which is a pH-dependent reaction unlike the coordinative dissolution. If possibility (1) holds, the hydroxylation is expected to proceed only when $E_{fb} + h\nu$ is more positive than $E_{Au(OH)_3/Au}$ ($E_{fb} + h\nu > 1.36 - 0.059$ pH V). Whereas if possibility (2) holds, Au NPs would be hydroxylated when the $E_{Au(OH)_3/Au}$ value is less positive than a value roughly equal to $E^\circ_{[AuCl_4]^-/Au}$.

Au NPs (ca. 40 nm) were prepared by malate reduction[23] and adsorbed on bare ITO electrodes, or those coated with

[*] Dr. H. Nishi, Prof. T. Tatsuma
Institute of Industrial Science, University of Tokyo
Komaba, Meguro-ku, Tokyo 153-8505 (Japan)
E-mail: tatsuma@iis.u-tokyo.ac.jp

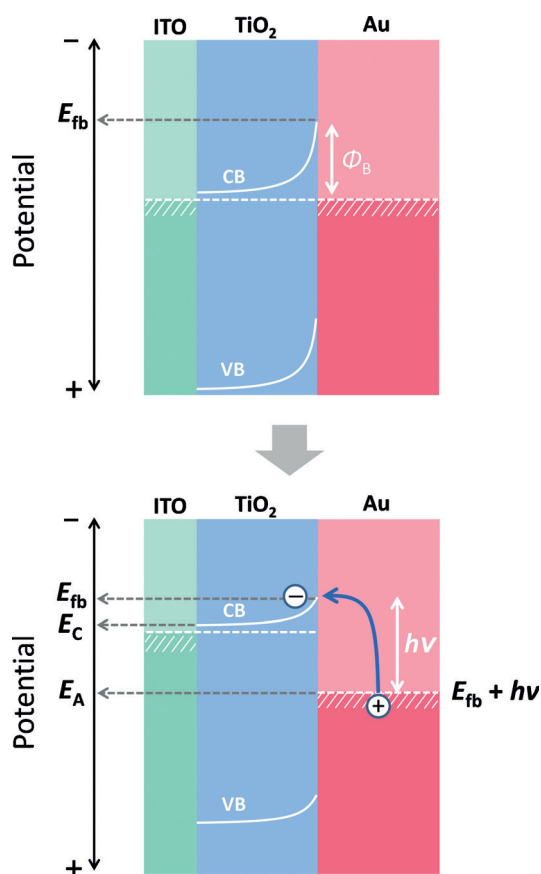The ORCID identification number(s) for the author(s) of this article can be found under http://dx.doi.org/10.1002/anie.201605914.

Figure 1. Band structure for PICS. Key: conduction (CB) and valence (VB) bands of TiO$_2$, flat band potential of TiO$_2$ (E_{fb}), cathodic (E_c) and anodic (E_A) potentials of PICS, Schottky barrier height (ϕ_B), and irradiated photon energy ($h\nu$).

Figure 2. a) Extinction spectrum and b) typical scanning electron micrographs of the TiO$_2$ electrode modified with Au NPs. c) CV of the ITO electrode modified with Au NPs in 0.5 M KNO$_3$ (pH 5.7). The inset shows a relationship between the applied potential and the extinction peak wavelength. d) Difference spectrum of the electrode obtained by subtracting the spectrum at 0.5 V from that at 1.5 V.

TiO$_2$, by spray pyrolysis.[24] Figure 2a shows an extinction spectrum and Figure 2b shows scanning electron micrographs of the Au NPs on TiO$_2$. The peak at 540 nm and the broad extinction at > 600 nm may be attributed to isolated and aggregated NPs seen in the micrograph, respectively. These assignments are supported by spectral simulations as discussed below.

The ITO electrodes modified with Au NPs were subjected to spectroelectrochemical measurements in order to determine the spectral changes caused by surface hydroxylation of the NPs. The extinction spectrum of NPs on the ITO electrode is similar to that on TiO$_2$. Results of the measurements at pH 5.7 are shown in Figure 2c. The cyclic voltammogram (CV) is similar to a typical CV for Au electrodes.[25–28] Oxidative formation and re-reduction of Au(OH)$_3$ are observed at a more positive and negative potential than 1.1 V (vs. NHE), respectively. Faradaic currents for Au oxidation are negligible in the more negative potential range. The threshold potential corresponds to the Au(OH)$_3$ formation potential in the Pourbaix diagram ($E_{Au(OH)_3/Au}$ = 1.03 V at pH 5.7). Although it is known that the potential is more negative for NPs smaller than 10 nm,[29] that for NPs of approximately 40 nm diameter is close to that for bulk Au. The LSPR peak at about 530 nm for isolated Au NPs is red-shifted as the potential is positively shifted from 0.5 to 1.1 V
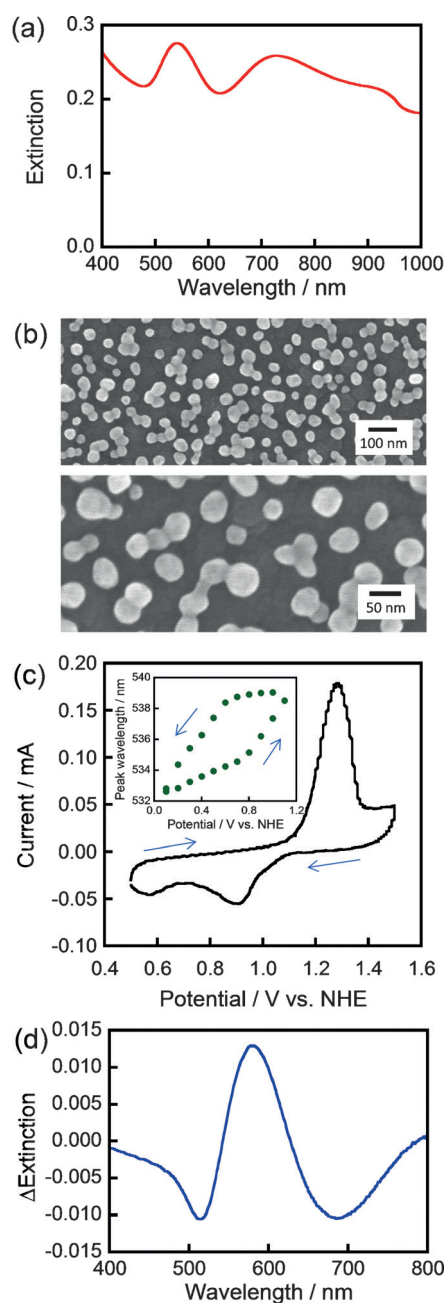
because of electrostatic charging.[30–32] The peak is further red-shifted at a more positive potential than 1.1 V because the particles are covered with dielectric Au(OH)$_3$.[28] The spectrum is initialized after re-reduction and electrostatic discharging of the NPs. In the difference spectrum (Figure 2d), a dip and a peak are formed at approximately 520 and 600 nm, respectively, as a result of the hydroxylation. The dip at about 700 nm can be assigned to a spectral shift of the aggregated NPs, as described below.

Subsequently, Au NPs on TiO₂ were irradiated with visible light. Figure 3a shows difference spectra after irradiation at 700, 800, 900, and 1000 nm (full-width at half maximum = 12 nm, the number of photons is approximately 2×10^{16} cm^{-2} s^{-1}) for 1 h in 0.5 M KNO₃ (pH 5.7). The baseline at 400–450 nm of each difference spectrum was adjusted to zero. The spectral shapes are similar to that for electrochemical hydroxylation (Figure 2d), indicating that the NP surface is hydroxylated. It is noteworthy that the spectral dip wavelengths in Figure 3a are roughly equal to the irradiation wavelengths. Similar wavelength selective oxidation reactions have been observed for oxidative dissolution of Ag NPs[15,16,33] and coordinative dissolution of Au NPs[17,20] based on PICS. We consider that the wavelength-selective dip formation is due to PICS by aggregated NPs. More specifically, electrons are injected selectively from resonant aggregates into the TiO₂ conduction band and are mainly consumed by reduction of ambient O₂,[4] whereas the positive charges left on the aggregated NPs lead to hydroxylation of the resonant aggregates.

To reproduce those difference spectra, we carried out finite-difference time-domain (FDTD) calculations for longitudinal LSPR extinction of NP dimer models (Figure 3b). The longitudinal mode is based on electron oscillation along the long axis of a dimer. Before hydroxylation, the dimer exhibits an extinction peak at a different wavelength, depending on the degree of fusion or contact of the NPs (Figure 3b). The broad extinction at >600 nm in Figure 2a would be reproduced by summation of these spectra. Assuming that hydroxylation converts the 1 nm thick surface layer of a Au particle into a 1.4 nm thick dielectric layer (the refractive index value of which is 2), the calculated longitudinal LSPR peak is red-shifted and thereby the difference spectrum gives a dip and a peak (Figure 3c). Upon irradiation with monochromatic light, PICS selectively occurs at dimers that resonate with the light, resulting in formation of a dip and a peak at around the irradiation wavelength and at a longer wavelength, respectively. The latter peak is not necessarily clear in Figure 3a because of detector switchover noise at 900 nm. In the electrochemical hydroxylation, the broad dip forms at about 700 nm (Figure 2d) because extinction is relatively high at around 700 nm in the initial spectrum (Figure 2a). The extinction peak derived from the transverse LSPR mode of the dimer, in which electrons oscillate along the short axis, is also red-shifted by oxidation because the longitudinal PICS. This results in the formation of a spectral dip and peak at approximately 520 and 600 nm, respectively (Figure 3a).

We performed similar experiments at pH 1.1, 2.6, and 9.8 (pH was adjusted by HNO₃ or KOH) and plotted the depth of the wavelength-selective dip in the difference spectra against the photon energy of irradiated light (Figure 3d). The minimum photon energy required for the reaction (that is, energy threshold of the hydroxylation) is determined by extrapolation to be about 1.05 eV (ca. 1180 nm) at all the pH values examined. In our previous study on coordinative dissolution of Au NPs,[20] the reaction proceeded when $E_{fb} + h\nu$ was close to, or more positive than, the potential for coordinative dissolution (that is, $E_{fb} + h\nu \geq E_{[AuCl_4]^-/Au}$).
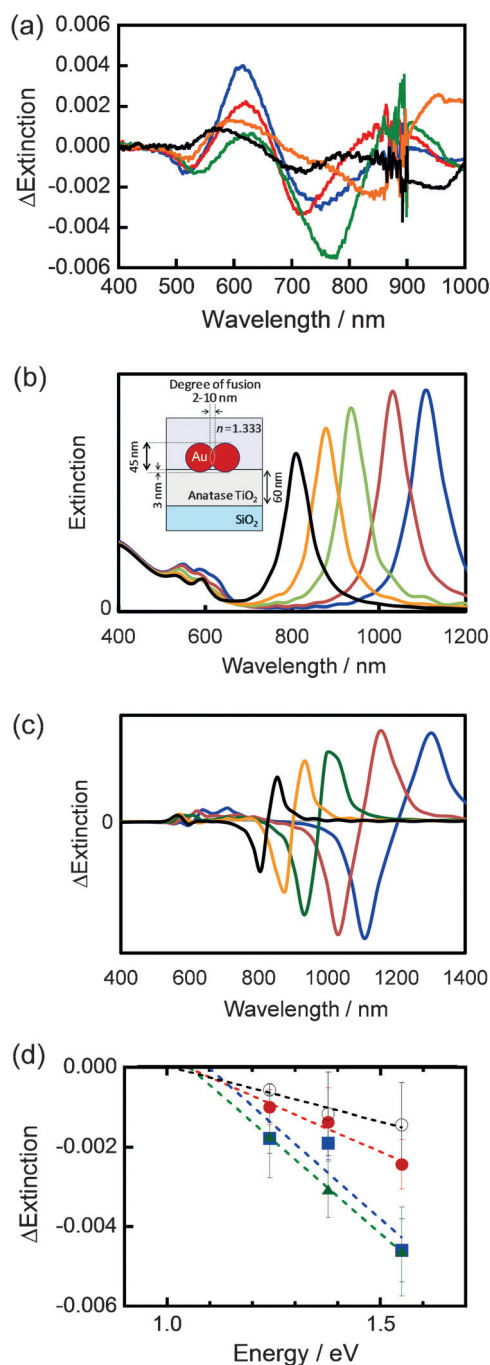

Figure 3. a) Difference spectra of the TiO₂ electrode modified with the Au NPs after monochromatic light illumination (600–1000 nm). Key: 600 nm (blue), 700 nm (red), 800 nm (green), 900 nm (orange), 1000 nm (black). b) Extinction spectra of the Au NP dimer models depicted in the inset, calculated by a FDTD method. c) Calculated difference spectra of the dimer models after surface hydroxylation of the NPs (see text for further detail). Key for (b) and (c), degree of fusion of two NPs: 2 nm (blue), 3 nm (red), 5 nm (green), 7 nm (yellow), 10 nm (black). d) Relationships between the photon energy of irradiated light and the depth of the wavelength-selective spectral dip. Key: pH 5.7 (green triangle), pH 2.6 (blue square), pH 1.1 (red circle), pH 9.8 (open circle).

Meanwhile, the electrode potential for hydroxylation of Au is given by $E_{Au(OH)_3/Au} = 1.36 - 0.059\,pH$,[22] which is plotted in
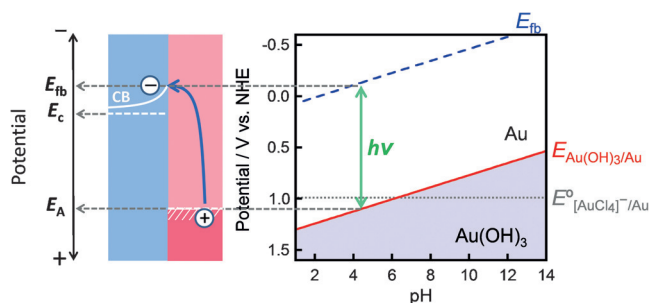
Figure 4. Pourbaix diagram for the Au–H$_2$O system and the corresponding band diagram.

the Pourbaix diagram (Figure 4, solid line; activities of solids are assumed to be unity). In the present study, the hydroxylation is induced by a photon with energy of > 1.05 eV, regardless of the pH value. If $h\nu$ is approximately equal to 1.05 eV, $E_{fb} + h\nu$ is about $1.17 - 0.059$ pH because $E_{fb} = 0.123 - 0.059$ pH for the present TiO$_2$. Thus, $E_{fb} + h\nu$ is close to $E_{Au(OH)_3/Au}$. In the experiments, the $E_{Au(OH)_3/Au}$ value is most likely more negative than $1.36 - 0.059$ pH because the activity of the thin Au(OH)$_3$ layer should be less than unity. Both of the previous and the present results can be explained if the anodic potential for PICS is about $E_{fb} + h\nu$ (possibility (1) mentioned above holds). The present results eliminate the other possibility, that holes generated at a certain defect level at a more positive potential than $E^{\circ}_{[AuCl_4]^-/Au}$ (which is independent of pH (Figure 4, dotted line)) are responsible for the oxidation of Au NPs (possibility (2)).

Considering the results described above, the oxidation ability of PICS in the previous and the present studies can be expressed by a schematic band structure shown in Figure 1. When a Au NP in contact with TiO$_2$ resonates with a photon with energy of $h\nu$ (which is higher than ϕ_B) at the interface between Au and TiO$_2$, an electron in the Au NP is injected into the TiO$_2$ conduction band by an external photoelectric effect, hot electron injection, or interfacial electron transition.[4–7,21,34,35] As a result of the electron transfer, TiO$_2$ works as the photocathode. If reduction at TiO$_2$ is sufficiently slow, electrons are accumulated and the photocathode potential (E_C) approaches the conduction band edge potential, which is E_{fb}. The electron transfer also results in loss of electrons in the Au NP, which acts as the photoanode. When oxidation at Au is slow enough, the photoanode potential (E_A) shifts positively from that in the dark. Thus, the ϕ_B value ($\phi_B = E_A - E_{fb}$) increases and finally approaches $h\nu$ in the ideal situation (note that ϕ_B should be less than $h\nu$ for electron transfer). Therefore, the maximum oxidation ability given by PICS (E_A) is considered to be about $E_{fb} + h\nu$.

Our conclusion is consistent with previous results reported elsewhere. For instance, the photon energy threshold of water oxidation into O$_2$, based on PICS, is reportedly in the range 1.08–1.46 eV at Au nanorods fabricated on Nb-doped TiO$_2$ with an E_{fb} of -0.40 V.[12] The value of $E_{fb} + h\nu$ is therefore 0.68–1.06 V, which agrees with the water oxidation potential under the experimental conditions ($E_{O_2/H_2O} = 0.82$ V).

In summary, a hydroxylation reaction based on PICS of Au NPs deposited on TiO$_2$ was investigated at different pH values and irradiation wavelengths. As a result, we found that the present results and our previous results for coordinative dissolution of Au can be explained systematically if the potential of the NPs equals $E_{fb} + h\nu$ ($E_A = E_{fb} + h\nu$). This might not necessarily hold for all PICS systems; in cases where a discrete level is formed on the plasmonic NP surface E_A could be determined by the level. However, in cases such as oxygen generation from water, which may proceed via Au oxides/hydroxides,[28] the present finding is extremely important for designing overall photocatalytic reactions.

[1] S. Link, M. A. El-Sayed, *J. Phys. Chem. B* **1999**, *103*, 8410–8426.
[2] H. A. Atwater, A. Polman, *Nat. Mater.* **2010**, *9*, 205–213.
[3] S. K. Cushing, J. Li, F. Meng, T. R. Senty, S. Suri, M. Zhi, M. Li, A. D. Bristow, N. Wu, *J. Am. Chem. Soc.* **2010**, *134*, 15033–15041.
[4] Y. Tian, T. Tatsuma, *J. Am. Chem. Soc.* **2005**, *127*, 7632–7637.
[5] Y. Takahashi, T. Tatsuma, *Appl. Phys. Lett.* **2011**, *99*, 182110.
[6] M. W. Knight, H. Sobhani, P. Nordlander, N. J. Halas, *Science* **2011**, *332*, 702–704.
[7] P. Reineck, G. P. Lee, D. Brick, M. Karg, P. Mulvaney, *Adv. Mater.* **2012**, *24*, 4750–4755.
[8] E. Kowalska, R. Abe, B. Ohtani, *Chem. Commun.* **2009**, 241–243.
[9] H. Kominami, A. Tanaka, K. Hashimoto, *Chem. Commun.* **2010**, *46*, 1287–1289.
[10] Y. Ide, M. Matsuoka, M. Ogawa, *J. Am. Chem. Soc.* **2010**, *132*, 16762–16764.
[11] C. Gomes Silva, R. Juáez, T. Marino, R. Molinari, H. García, *J. Am. Chem. Soc.* **2011**, *133*, 595–602.
[12] Y. Nishijima, K. Ueno, Y. Kotake, K. Murakoshi, H. Inoue, H. Misawa, *J. Phys. Chem. Lett.* **2012**, *3*, 1248–1252.
[13] A. Tanaka, S. Sakaguchi, K. Hashimoto, H. Kominami, *ACS Catal.* **2013**, *3*, 79–85.
[14] A. Tanaka, K. Nakanishi, R. Hamada, K. Hashimoto, H. Kominami, *ACS Catal.* **2013**, *3*, 1886–1891.
[15] Y. Ohko, T. Tatsuma, T. Fujii, K. Naoi, C. Niwa, Y. Kubota, A. Fujishima, *Nat. Mater.* **2003**, *2*, 29–31.
[16] K. Naoi, Y. Ohko, T. Tatsuma, *J. Am. Chem. Soc.* **2004**, *126*, 3664–3668.
[17] Y. Konishi, I. Tanabe, T. Tatsuma, *Chem. Commun.* **2013**, *49*, 606–608.
[18] T. Tatsuma, K. Takada, T. Miyazaki, *Adv. Mater.* **2007**, *19*, 1249–1251.
[19] T. Tatsuma, Y. Katagi, S. Watanabe, K. Akiyoshi, T. Kawawaki, H. Nishi, E. Kazuma, *Chem. Commun.* **2015**, *51*, 6100–6103.
[20] Y. Konishi, I. Tanabe, T. Tatsuma, *Dalton Trans.* **2013**, *42*, 15937–15940.

[21] E. Kazuma, T. Tatsuma, *Adv. Mater. Interfaces* **2014**, *1*, 1400066.

[22] G. H. Kelsall, N. J. Welham, M. A. Diaz, *J. Electroanal. Chem.* **1993**, *361*, 13–24.

[23] H. Nishi, S. Kobatake, *Dyes Pigm.* **2012**, *92*, 847–853.

[24] H. Nishi, T. Torimoto, T. Tatsuma, *Phys. Chem. Chem. Phys.* **2015**, *17*, 4042–4046.

[25] N. Tateishi, K. Nishimura, K. Yahikozawa, M. Nakagawa, M. Yamada, Y. Takasu, *J. Electroanal. Chem.* **1993**, *352*, 243–252.

[26] G. Tremiliosi-Filho, E. R. Gonzalez, A. J. Motheo, E. M. Belgsir, J.-M. Léger, C. Lamy, *J. Electroanal. Chem.* **1998**, *444*, 31–39.

[27] P. Rodriguez, M. T. M. Koper, *Phys. Chem. Chem. Phys.* **2014**, *16*, 13583–13594.

[28] O. Diaz-Morales, F. Calle-Vallejo, C. de Munck, M. T. M. Koper, *Chem. Sci.* **2013**, *4*, 2334–2343.

[29] W. J. J. Plieth, *Phys. Chem.* **1982**, *86*, 3166–3170.

[30] A. H. Ali, R. J. Luther, C. A. Foss, Jr., *Nanostruct. Mater.* **1997**, *9*, 559–562.

[31] T. Ung, M. Giersig, D. Dunstan, P. Mulvaney, *Langmuir* **1997**, *13*, 1773–1782.

[32] H. Nishi, S. Hiroya, T. Tatsuma, *ACS Nano* **2015**, *9*, 6214–6221.

[33] E. Kazuma, T. Tatsuma, *Nanoscale* **2014**, *6*, 2397–2405.

[34] A. Furube, L. Du, K. Hara, R. Katoh, M. Tachiya, *J. Am. Chem. Soc.* **2007**, *129*, 14852–14853.

[35] N. Sakai, Y. Fujiwara, Y. Takahashi, T. Tatsuma, *ChemPhysChem* **2009**, *10*, 766–769.